J Pharmacol Sci **95**, 81 – 93 (2004)

Journal of Pharmacological Sciences

Full Paper

Identification of Endogenous Surrogate Ligands for Human P2Y Receptors Through an In Silico Search

Takeshi Hiramoto[1], Yosuke Nonaka[1], Kazuko Inoue[1], Takefumi Yamamoto[2], Mariko Omatsu-Kanbe[3], Hiroshi Matsuura[3], Keigo Gohda[4], and Norihisa Fujita[1,*]

[1]*Laboratory of Pharmcoinformatics, Department of Bioscience and Biotechnology, College of Science and Engineering, Ritsumeikan University, Kusatsu, Shiga 525-8577, Japan*
[2]*Central Research Laboratory and* [3]*Department of Physiology, Shiga University of Medical Science, Ohtsu, Shiga 520-2192, Japan*
[4]*CAMM-Kansai, Higashinada, Kobe 658-0046, Japan*

Received February 2, 2004; Accepted March 18, 2004

Abstract. G protein-coupled receptors (GPCRs) are distributed widely throughout the human body, and nearly 50% of current medicines act on a GPCR. GPCRs are considered to consist of seven transmembrane α-helices that form an α-helical bundle in which agonists and antagonists bind. A 3D structure of the target GPCR is indispensable for designing novel medicines acting on a GPCR. We have previously constructed the 3D structure of human $P2Y_1$ ($hP2Y_1$) receptor, a GPCR, by homology modeling with the 3D structure of bovine rhodopsin as a template. In the present study, we have employed an in silico screening for compounds that could bind to the $hP2Y_1$-receptor model using AutoDock 3.0. We selected 21 of the 30 top-ranked compounds, and by measuring intracellular Ca^{2+} concentration, we identified 12 compounds that activated or blocked the $hP2Y_1$ receptor stably expressed in recombinant CHO cells. 5-Phosphoribosyl-1-pyrophosphate (PRPP) was found to activate the $hP2Y_1$ receptor with a low ED_{50} value of 15 nM. The Ca^{2+} assays showed it had no significant effect on $P2Y_2$, $P2Y_6$, or $P2X_2$ receptors, but acted as a weak agonist on the $P2Y_{12}$ receptor. This is the first study to rationally identify surrogate ligands for the P2Y-receptor family.

Keywords: G protein-coupled receptor, $P2Y_1$ receptor, in silico screening, AutoDock, 5-phosphoribosyl-1-pyrophosphate

Introduction

The rhodopsin family is an important class of G protein-coupled receptors (GPCRs) that have crucial roles in many signal transductions. From a therapeutic point of view, GPCRs represent one of the most critical classes of confirmed drug targets, since nearly 50% of all contemporary medicines act on a GPCR (1). However, as a membrane-bound protein such as a GPCR is not readily crystallized, only a couple of GPCR-type receptors, bovine rhodopsin and bacteriorhodopsin, have had their 3D structures clarified. The reported model of bovine rhodopsin includes 194 residues that form seven transmembrane (TM) α-helices (2). This model offered a structural template for other GPCRs, including assignment of the location of highly conserved amino acids. In addition, several novel methods to predict the configuration of GPCRs have recently been proposed (3 – 8). We have previously constructed the 3D structure of the human $P2Y_1$ receptor, a GPCR, by a hybrid approach, based on the high-resolution X-ray structure of rhodopsin, and Fourier transform analysis for α-helix prediction (9, 10). The 3D model of the $hP2Y_1$ receptor showed good agreement with the pharmacophore features of the agonist, ADP.

A number of computer docking software have been utilized successfully to fulfill the purpose of the computer-based drug design. This type of software is useful in evaluating the binding mode of candidate ligands or drug molecules to target macromolecules

*Corresponding author. FAX: +81-77-561-5203
E-mail: nori@is.ritsumei.ac.jp

such as nucleic acids and enzymes. In the drug design, an experimental structure for a target protein complexing with a ligand can allow us to examine the details of the binding site and to design de novo compounds. AutoDock (11 – 13) has a ligand mobilized by a genetic algorithm method and evaluates rapid grid-based energy. Previous applications of AutoDock 3.0 include the prediction of substrate binding to enzymes (14), computer-aided drug design of non-peptide inhibitors of HIV protease (15), and molecular modeling of interactions of non-peptide antagonist with the human vasopressin V_{1a} and V_2 receptors and with oxytocin receptors (16). The study of human vasopressin and oxytocin receptors showed good agreement with the molecular affinity data and suggested that AutoDock 3.0 is a useful tool for docking a compound to a GPCR model.

The $P2Y_1$ receptor, cloned in 1993, belongs to the purinoceptor subfamily which is classified into two pharmacologically distinct families of P2Y receptor and P2X-receptor classes (17, 18). P2Y receptors are members of the superfamily of rhodopsin-like GPCRs. The classification of P2Y receptors based on the primary sequences deduced from cDNAs divides them into ten kinds of subclasses: $P2Y_1$, $P2Y_2$, $P2Y_3$, $P2Y_4$, $P2Y_6$, $P2Y_8$, $P2Y_{11}$, $P2Y_{12}$, $P2Y_{13}$, and $P2Y_{14}$ (19 – 21). However, these subclasses of P2Y receptors are considerably confused due to the lack of specific agonist and antagonist for each subtype. Thus the effort to discover a specific agonist and antagonist for each P2Y receptor is an urgent subject for the elucidation of their physiological functions. Recently, $P2Y_1$ and $P2Y_{12}$ receptors have been proposed as potential therapeutic targets for thrombosis.

Therefore, using AutoDock 3.0, we have conducted an in silico screening for compounds that could bind to $hP2Y_1$ receptor. To confirm the results of the in silico screening, we measured the abilities of the selected compounds to stimulate intracellular Ca^{2+} concentration ($[Ca^{2+}]_i$) increase in the CHO cells transfected with the $hP2Y_1$-receptor gene. The aim of this study is to rationally discover surrogate compounds for $hP2Y_1$ receptor by employing in silico and in vitro approaches.

Materials and Methods

In silico screening using the AutoDock 3.0

We have previously constructed the 3D structure of $hP2Y_1$ receptor by Fourier transform analysis and homology modeling with the bovine rhodopsin 3D structure as a template (10). To search for $hP2Y_1$ agonists and antagonists, we used the 3D model of the $hP2Y_1$ receptor as a template for in silico screening. We used AutoDock 3.0, a ligand flexible docking program (11 – 13), according to the manufacturer's instructions with our in-house database, which includes animal metabolites. The number of grid points in the x, y, z-axis was 60 × 60 × 60 with grid points separated by 0.375 Å. Docking runs were performed using the Larmarckian genetic algorithm. The population size was set to 50. Each docking experiment consisted of a series of 200 simulations. The resulting initial set of 200 receptor-ligand configurations included crude configurations and required further refinement. To this end, the top 10 configurations of binding energy as ranked by AutoDock were energy-minimized (1000 steps of conjugate gradients method) with the CHARMm force field in the standard condition that all Cα carbon positions were fixed and the dielectric value was 4.0. These energy-minimizations were calculated using the InsightII/CHARMm programs (Accelrys, San Diego, CA, USA), and the lowest-energy configuration was selected. A total of 500 compounds in our database were calculated as ligands by this method, including animal metabolites such as carbohydrates, fatty acids, steroids, amino acids, amines, nucleic acids, and vitamins. Our 3D compound database was based on the 2D molecules in KEGG LIGAND database (http://www.genome.ad.jp/ligand/). These 2D molecules were converted to 3D and energy-minimized using the InsightII/CHARMm programs.

Cell culture

The CHO-K1 (Chinese Hamster ovary) cell line was used to generate the Flp-In™ CHO cell line (Invitrogen Carlsbad, CA, USA). The Flp-In™ CHO cell line contains a single Flp Recombination Target (FRT) site that has a mutated SV40 early promoter. The location of the FRT site in the Flp-In™ CHO cell line has not been mapped, but has been demonstrated to have integrated into a highly transcriptionally active genomic locus. Flp-In™ CHO cells were maintained in Ham's F-12 medium (Invitrogen) supplemented with 100 unit /ml penicillin, 100 μg/ml streptomycin, 100 μg/ml zeocin, 2 mM L-glutamine, and 10% fetal bovine serum (FBS) at 37°C in a CO_2 incubator with 5% CO_2.

Construction of $hP2Y_1$-Gqα fusion protein and $hP2Y_2$-Gqα fusion protein

The $hP2Y_1$-Gqα DNA was generated by a two-step PCR protocol using Pfu polymerase, Pyrobest (Toyobo, Osaka). A set of fusion primers (sense and antisense) was synthesized with 16 bp from the C-terminus of the $hP2Y_1$ receptor, 18 bp encoding a hexahistidine tag, and 16 bp from the N-terminus of human Gqα (hGqα). In the first PCR, the $hP2Y_1$-receptor gene in pcDNA3

served as a template to amplify the sequence between a sense primer designed for the N-terminus of the $hP2Y_1$ receptor and the antisense fusion primer. In the second PCR, the hGqα gene in PUC18 served as a template to amplify the gene between the sense fusion primer and the antisense primer for the C-terminus of hGqα. Then, the $hP2Y_1$-Gqα fusion gene was synthesized by a further PCR with the products of the first and second PCR as templates and the sense primer of the *Bam*HI site in the $hP2Y_1$ sequence and the antisense primer in the extra *Bam*HI site in hGqα sequence. This fragment was digested with *Bam*HI and cloned into the Flp-In™ System expression vector, pcDNA5/FRT.

The $hP2Y_2$-hGqα fusion gene was generated by the similar method as mentioned above using specific primers of the $hP2Y_2$-receptor sequence. The fragment of the $hP2Y_2$-hGqα gene was digested with *Bam*HI and cloned into the vector pcDNA5/FRT. The accuracy of all PCR-derived sequences was confirmed by the DNA sequence-analyses using the ABI PRISM 3100 Genetic Analyzer (Applied Biosystems, Foster City, CA, USA).

Generation of stably transfected cell lines

Purified plasmid DNA (1 μg) containing the $hP2Y_1$-hGqα or $hP2Y_2$-hGqα gene was stably transfected into Flp-In™ CHO cells using Lipofectamine™ 2000 (Invitrogen) in a final volume of 100 μl of Opti-MEM reagent (Invitrogen). After transfection, cell populations stably expressing these genes were obtained by selection with 0.5 mg/ml hygromycin B (Invitrogen). Clonal cell lines were isolated, and the expression of $hP2Y_1$-hGqα fusion protein and $hP2Y_2$-hGqα fusion protein were confirmed by the RT-PCR method and Western blotting.

RT-PCR

Total RNA was isolated from wild-type CHO cells and from CHO cells engineered to express the $hP2Y_1$-hGqα or $hP2Y_2$-hGqα fusion protein using the TRIzol reagent (Invtrogen). Total RNA isolated from each cell line (1 – 3 μg) was used to perform reverse transcription by the reverse transcriptase ReverTra Ace (Toyobo). PCR amplification was done with: i) primer 1 (5-cccac cggtacagcggtgtgg-3) and primer 2 (5-tactcttgccactctctc ctg-3), suitable to amplify the 856 bp spanning region of $hP2Y_1$-hGqα; or ii) primer 3 (5-'gagctcttcagccgcttcgtg-3) and primer 2, suitable to amplify the 737 bp region of $hP2Y_2$-hGqα (Fig. 1). The DNA size-standard was 100 bps ladder marker (Toyobo).

We also investigated which subtypes were expressed in wild-type CHO cells by RT-PCR. PCR amplification was done with primers suitable to amplify the 200 – 700-bp spanning regions of the P2Y-receptor family ($P2Y_1$, $P2Y_2$, $P2Y_4$, $P2Y_6$, $P2Y_{12}$).

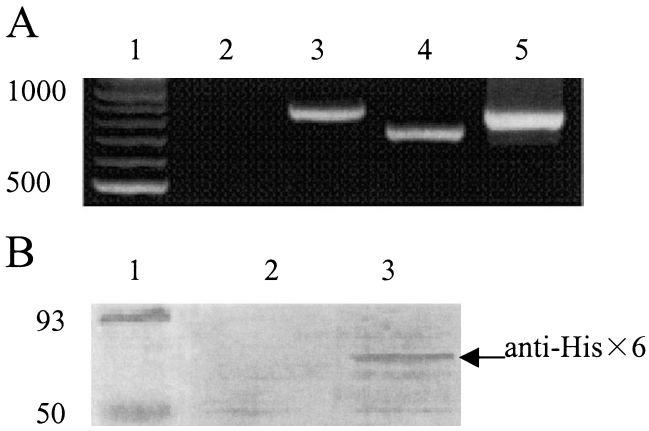

Fig. 1. Detection of the expressed $hP2Y_1$-hGqα fusion protein in transfected CHO cells. A) RT-PCR analysis: DNA products by RT-PCR from wild-type CHO cells (lane 2), transfected cells stably expressing $hP2Y_1$-hGqα (lane 3), or $hP2Y_2$-hGqα (lane 4). Primers specific for the $hP2Y_1$-hGqα gene (lanes 2 and 3), the $hP2Y_2$-hGqα gene (lane 4) or the β-actin gene (lane 5) were used. The DNA size standard is 100-bp ladder marker (1000 to 500 bp in lane 1). B) Western blotting analysis: proteins extracted from wild-type CHO cells (lane 2) or cells stably expressing $hP2Y_1$-hGqα (lane 3). $hP2Y_1$-hGqα protein was detected by anti-His×6 antibody (lanes 2, 3). Lane 1 contains protein molecular weight marker (93 and 50 kDa).

Western blotting

Membrane samples from wild-type and stably transfected CHO cells were separated on 10% SDS polyacrylamide gels. Following electrophoresis, proteins were transferred to nitrocellulose and reacted with hexahistidinetag antibody (1:4000). Immunoreactive bands were visualized by sheep anti-mouse IgG conjugated with horseradish peroxidase, using 3,3-diaminobenzidine tetrahydrochloride (DAB) and H_2O_2 as substrates.

$[Ca^{2+}]_i$ measurements

The $[Ca^{2+}]_i$ increase was measured using the Ca^{2+} indicator fura-2/AM (Calbiochem, San Diego, CA, USA) in the wild-type and stably transfected CHO cells perfused with the standard bath solution consisting of Krebs-Ringer bicarbonate Hepes (KRBH) buffer supplemented with 5.6 mM glucose and 0.05% BSA. The cells were loaded with membrane permeant fura-2/AM (5 μM) in the dark for 40 min in a standard bath solution. Fura-2-loaded cells were then incubated in the standard bath solution for 30 min at 37°C and transferred to the recording chamber mounted on the stage of an inverted microscope (IX70; Olympus, Tokyo). The recording chamber was maintained at 37°C and was perfused continuously at a rate of 1.5 ml/min with the standard bath solution or some

test solutions. The fluorescence measurement of $[Ca^{2+}]_i$ increase was performed using a microspectrofluorometer (Lambda DG4). All nucleotides or nucleotide analogues used were from Sigma (St. Louis, MO, USA).

Results

In silico screening using AutoDock 3.0

To test if AutoDock screening can identify known potential $hP2Y_1$ ligands, we added known $P2Y_1$ agonists [ADP, 2-methylthioADP (2MeSADP), 2-methylthio-ATP (2MeSATP), and ATPγS] and antagonists [adenosine 3-phosphate 5-phosphate (A3P5P), adenosine 3-phosphate 5-phosphosulfate (A3P5PS), N^6-methyl-2'-deoxyadenosine-3',5'-bisphosphate (MRS2179), and pyridoxal-phosphate-6-azophenyl-2',4'-disulfonic acid (PPADS)] to the database. These results showed all the added ligands were calculated to have significantly low binding energies. The binding energy values of added ligands were between −15.07 and −11.68 kcal/mol, while those of other neurotransmitters are −2.39 kcal/mol for acetylcholine, −5.31 kcal/mol for dopamine, and −3.89 kcal/mol for GABA. Since those known $hP2Y_1$ ligands were ranked within the top 30 by the AutoDock, a total of 30 compounds were evaluated as hits satisfying the requirement that each calculated binding energy was less than −11.68 kcal/mol (Table 1).

Detection of the expressed $hP2Y_1$-hGqα and $hP2Y_2$-hGqα fusion protein

We confirmed the expression of $hP2Y_1$-hGqα and $hP2Y_2$-hGqα fusion protein in stably transfected CHO cells by the RT-PCR method. Amplification of $hP2Y_1$-hGqα and $hP2Y_2$-hGqα fusion protein resulted in single bands around the predicted sizes of 856 and 737 bp (Fig. 1A, lanes 3 and 4). We also confirmed the expression of $hP2Y_1$-hGqα fusion protein by Western blotting by using anti-His×6 antibody (Fig. 1B). Western blotting showed 80-kDa specific bands in lane 3 containing proteins extracted from stably transfected CHO cells.

Table 1. Results of docking simulation using AutoDock 3.0

	Ligand	AutoDock energy (kcal/mol)		Ligand	AutoDock energy (kcal/mol)
1	XTP	−15.93	26	**GDP**	−12.33
2	Adenosine 5'-tetraphosphate	−15.81	27	MRS2179	−12.28
3	**Farnesyl diphosphate**	−15.68	28	**UDP**	−12.21
4	**PRPP**	−15.33	29	**D-Fructose 1,6-bisphosphate**	−12.05
5	**GTP**	−15.17	30	**PPADS**	−11.68
6	**A3P5PS**	−15.07	31	RDP	−11.33
7	**UTP**	−15.07	32	**D-Fructose 2,6-bisphospahate**	−11.10
8	RTP	−14.83	33	IMP	−10.87
9	ADP-ribose 2'-phosphate	−14.69	34	ADP-glucose	−10.86
10	**UDP-glucose**	−14.66	35	CMP	−10.78
11	**2MeSATP**	−14.65	36	alpha-Tocopherol	−10.72
12	**TTP**	−14.64	37	Thyrotropin-releasing hormone	−10.62
13	**2MeSADP**	−14.44	38	Cholesterol	−10.52
14	**CTP**	−14.44	39	XMP	−10.44
15	**ITP**	−14.39	40	D-Fructose 6-phosphoric acid	−10.40
16	**ATP**	−14.34	41	Deoxycholic acid	−10.22
17	A2P5P	−13.76	42	Leukotriene B_4	−10.21
18	Geranylgeranyl diphosphate	−13.71	43	Retinal	−10.00
19	**ATPγS**	−13.45	44	Ergosterol	−9.99
20	XDP	−13.21	45	RMP	−9.85
21	A3P5P	−12.88	46	Riboflavin	−9.75
22	**TDP**	−12.74	47	Creatine phosphate	−9.67
23	**CDP**	−12.65	48	**AMP**	−9.54
24	**ADP**	−12.59	49	GMP	−9.24
25	**IDP**	−12.33	50	UMP	−9.23

The top 50 compounds according to the AutoDock-binding energy are listed. The compounds shown as bold type were selected to the in vitro test of $[Ca^{2+}]_i$ measurement.

$[Ca^{2+}]_i$ measurements in CHO cells expressing $hP2Y_1$-$hGq\alpha$ fusion protein and $hP2Y_2$-$hGq\alpha$ fusion protein

We selected 21 commercially available compounds that were shown to have an AutoDock binding energy of less than −11.68 kcal/mol. Furthermore, two compounds, D-fructose 2,6-bisphosphate (−11.10 kcal/mol) and AMP (−9.54 kcal/mol) were selected as negative controls. These 23 compounds were subjected to the in vitro test of $[Ca^{2+}]_i$ measurement using the transfected CHO cells stably expressing $hP2Y_1$-$hGq\alpha$ fusion protein (shown as bold type in Table 1). The $hP2Y_1$ agonists, 2MeSADP, 2MeSATP, ADP, and ATPγS, evoked the $[Ca^{2+}]_i$ increase more effectively in the transfected cells than in the wild-type cells (Fig. 2: A – D). Additionally, we found that three compounds, PRPP (5-phosphoribosyl-1-pyrophosphate), CDP, and D-fructose 1,6-bisphosphate, evoked the $[Ca^{2+}]_i$ increase more effectively in the transfected cells (Fig. 2: E – G). Their stimulating actions were in a dose-dependent manner with a rank order of potency of 2MeSADP > 2MeSATP ≥ ADP ≥ ATPγS > PRPP ≫ CDP > D-fructose 1,6-bisphosphate. The ED_{50} values were 0.026 ± 0.0015 nM of 2MeSADP, 1.4 ± 0.07 nM of 2MeSATP, 2.2 ± 0.14 nM of ADP, 3.8 ± 0.10 nM of ATPγS, 15 ± 5.3 nM of PRPP, 6,500 ± 2,400 nM of CDP, and 14,000 ± 2,100 nM of D-fructose 1,6-bisphosphate. Each ligand evoked a similar maximum $[Ca^{2+}]_i$ increase. Other nucleic acids, ATP, TTP, GTP, CTP, UTP, ITP, TDP, GDP, UDP, IDP, AMP, and UDP-glucose, evoked the $[Ca^{2+}]_i$ increase in the transfected cells without any significant differences from the wild-type cells. AMP, farnesyl diphosphate, and D-fructose 2,6-bisphosphate did not show any appreciable effect at 1 – 100 μM in the transfected cells (data not shown). Then we investigated the effects of the P2 antagonists, 100 μM suramin and 1 μM PPADS, and also 10 μM of the putative $hP2Y_1$-specific antagonist A3P5PS on the 10 nM ADP-evoked $[Ca^{2+}]_i$ increase in the transfected cells. As a result, all of the antagonists significantly reduced the 10 nM ADP-evoked $[Ca^{2+}]_i$ increase (Fig. 3: A – C). Furthermore, 1 μM A3P5PS completely blocked the 100 nM PRPP-evoked $[Ca^{2+}]_i$ increase (Fig. 3H). In addition, 1 μM UDP and 100 μM UDP-glucose showed a weak antagonistic effect on the 10 nM ADP-evoked $[Ca^{2+}]_i$ increases (Fig. 3: D and E), while D-fructose 2,6-bisphosphate shows no appreciable effect on the 10 nM ADP-evoked $[Ca^{2+}]_i$ increase (Fig. 3F). The P1 agonist, adenosine at 100 μM had no effect on it (Fig. 3G).

In order to estimate the selectivity of PRPP action for P2Y receptors, we examined the activity of PRPP to stimulate $[Ca^{2+}]_i$ increases in the CHO cells expressing $hP2Y_2$-$hGq\alpha$ fusion proteins. ATP and UTP, known agonists for the $hP2Y_2$ receptor, evoked the $[Ca^{2+}]_i$ increase more effectively in the transfected cells than in the wild-type cells (Fig. 4: A and B). The ED_{50} values were 0.82 ± 0.033 nM of ATP and 16 ± 3.1 nM of UTP, and the maximum increases evoked by ATP and UTP were almost in the same level. However, PRPP showed only a weak $[Ca^{2+}]_i$ increase in the transfected cells as well as the wild-type cells. As seen in Fig. 4C, the ED_{50} values were estimated to be 400 ± 30 nM in both cell lines. CDP had no appreciable effect under the same assay conditions (Fig. 4D).

We also tested whether PRPP acted on P2X receptors. As differentiated PC12 cells (dPC12 cells) are known to express $P2X_2$ receptors that responds to extracellular nucleotides, we measured the $[Ca^{2+}]_i$ response in the cells. ATP and 2MeSATP showed long and dose-dependent $[Ca^{2+}]_i$ increases in the dPC12 cells through the activation of the $P2X_2$ receptors. In contrast, $P2X_2$ receptors did not respond to PRPP even at the concentration of 10 μM (data not shown).

Correlation between AutoDock energies and ED_{50} values of $[Ca^{2+}]_i$ measurements

Figure 5 shows a plot of the correlation between binding energies calculated by AutoDcok and the ED_{50} values of $[Ca^{2+}]_i$ measurements in the transfected CHO cells. Figure 5 uses the data of 2MeSADP, 2MeSATP, ADP, ATPγS, PRPP, CDP, and D-fructose 1,6-bisphosphate, which showed potency as $hP2Y_1$ agonists in Fig. 2. The straight line was drawn by the least-squares method. The correlation coefficient of the calculated binding energies and ED_{50} values was 0.63 (P<0.05).

3D models of $hP2Y_1$ receptor and agonists

We constructed a 3D model of ADP-bound $hP2Y_1$ receptor using the AutoDock program. This 3D model showed a lower energy of the ligand-bound $hP2Y_1$-receptor complex than the model we previously reported (10). The newly constructed model also shows good agreements with the pharmacophore feature of ADP. The model shows that the phosphate group of ADP interacts with Arg310/TM7 (2.07Å O2P) and Lys280 /TM6 (2.00Å O2P, 2.05Å O4P, 1.86Å O6P); the ribose of ADP interacts with Arg310/TM7 (1.84Å O5); and the adenine moiety interacts with Tyr111/TM2 (2.23Å N6H2) and Arg310/TM7 (2.27Å N3) (Fig. 6A). 2MeSADP, 2MeSATP, and CDP showed a similar docking manner to the $hP2Y_1$-ADP model (data not shown). In the case of PRPP, the 5-phosphate group of PRPP interacts with Gln307/TM7 (2.21Å O20) and Arg310/TM7 (1.90Å O14), while the ribose moiety interacts with Arg310/TM7 (2.44Å O2) and the 1-diphosphate group interacts with His132/TM3 (2.03Å O17), Lys280/TM6 (2.09Å O17, 1.91Å O18, 2.47Å

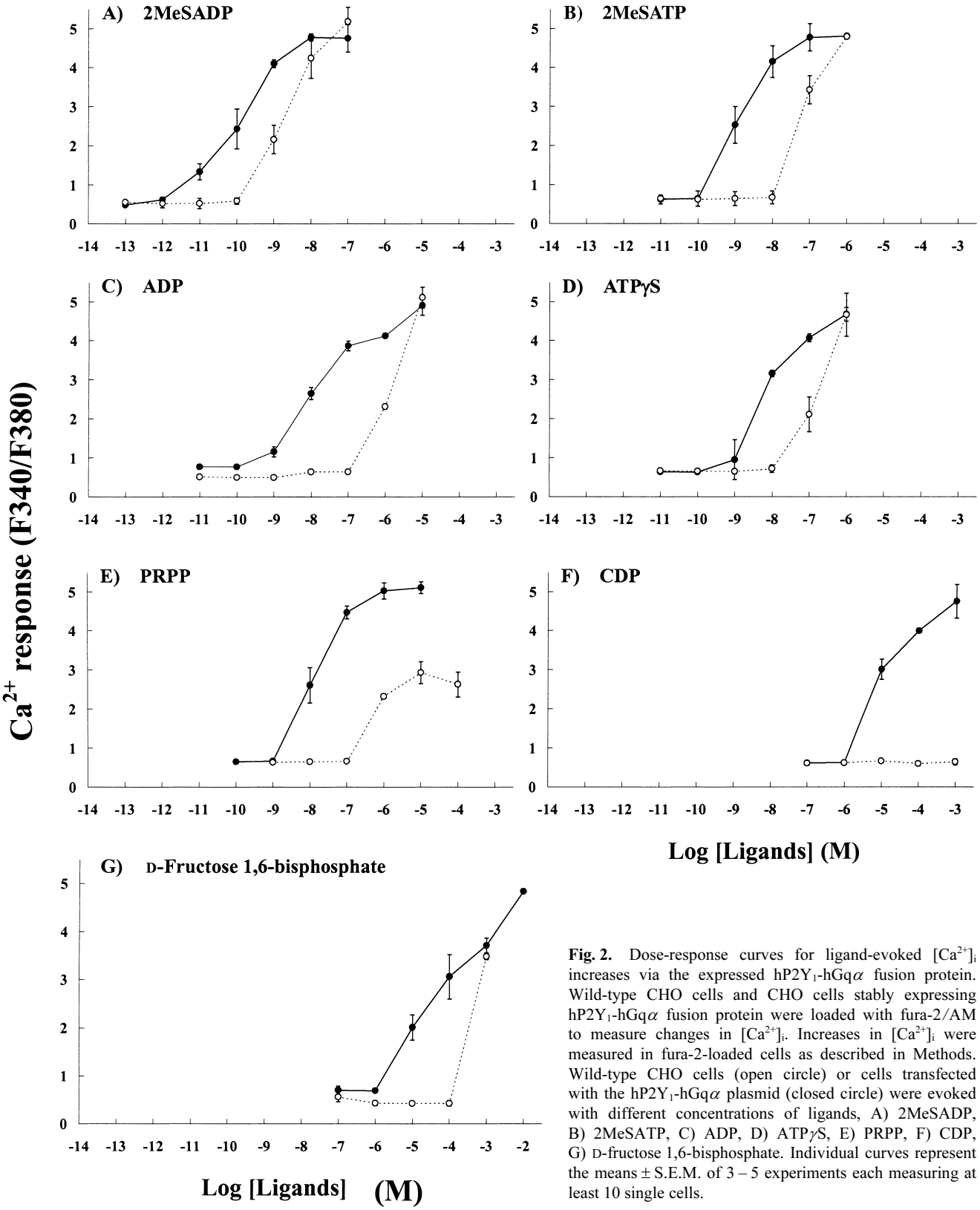

Fig. 2. Dose-response curves for ligand-evoked $[Ca^{2+}]_i$ increases via the expressed $hP2Y_1$-hGqα fusion protein. Wild-type CHO cells and CHO cells stably expressing $hP2Y_1$-hGqα fusion protein were loaded with fura-2/AM to measure changes in $[Ca^{2+}]_i$. Increases in $[Ca^{2+}]_i$ were measured in fura-2-loaded cells as described in Methods. Wild-type CHO cells (open circle) or cells transfected with the $hP2Y_1$-hGqα plasmid (closed circle) were evoked with different concentrations of ligands, A) 2MeSADP, B) 2MeSATP, C) ADP, D) ATPγS, E) PRPP, F) CDP, G) D-fructose 1,6-bisphosphate. Individual curves represent the means ± S.E.M. of 3 – 5 experiments each measuring at least 10 single cells.

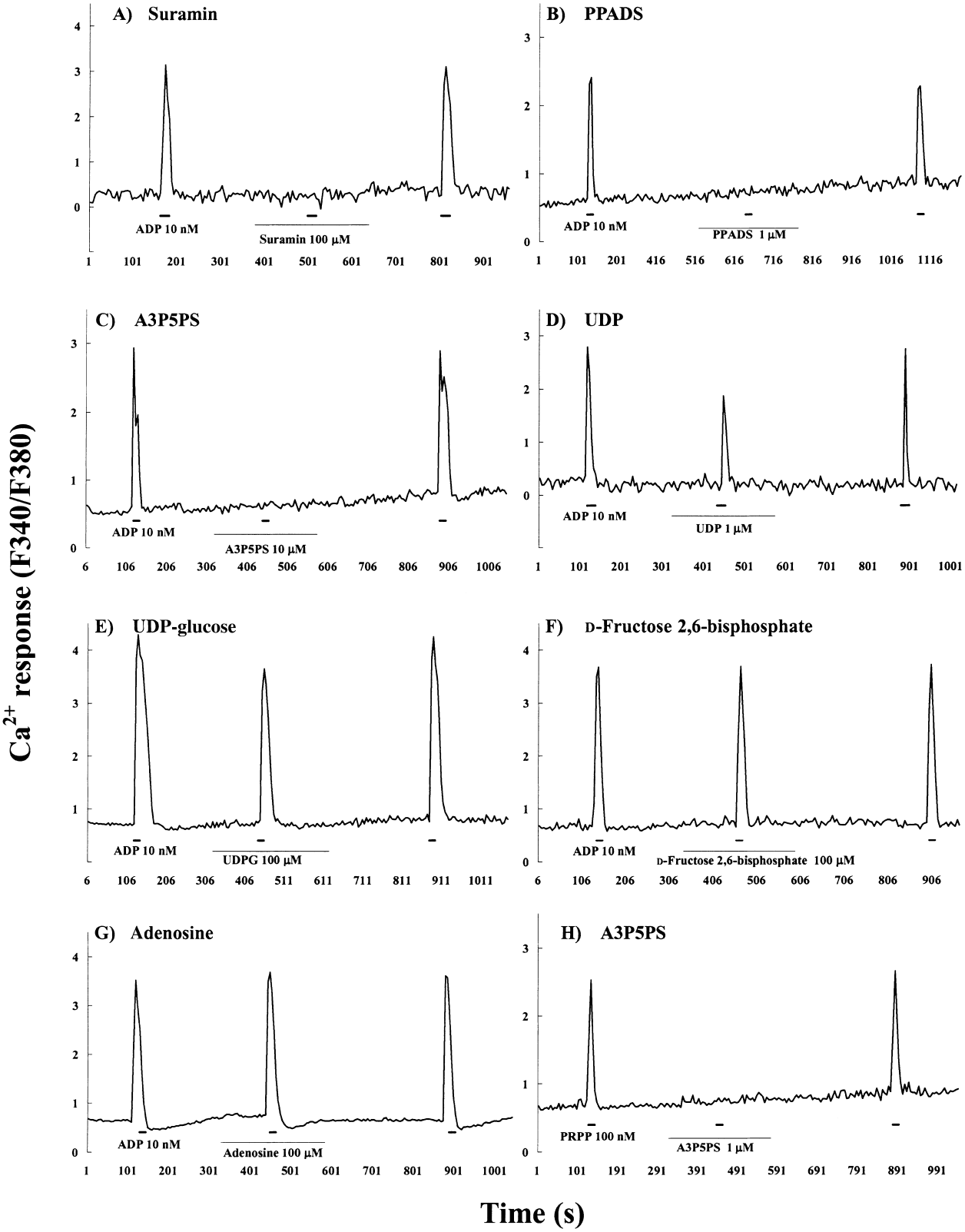

Fig. 3. Antagonistic effects of ligands on the ADP- and PRPP-evoked $[Ca^{2+}]_i$ increases. CHO cells stably expressing $hP2Y_1$-hGqα fusion protein were evoked with 10 nM ADP (A – G) or 100 nM PRPP (H) in the presence or absence of 100 μM suramin (A), 1 μM PPADS (B), 10 μM A3P5PS (C), 1 μM UDP (D), 100 μM UDP-glucose (E), 100 μM D-fructose 2,6-bisphosphate (F), 100 μM adenosine (G), and 1 μM A3P5PS (against PRPP) (H). Each ligand was added to the standard bath solution as indicated by the horizontal bars.

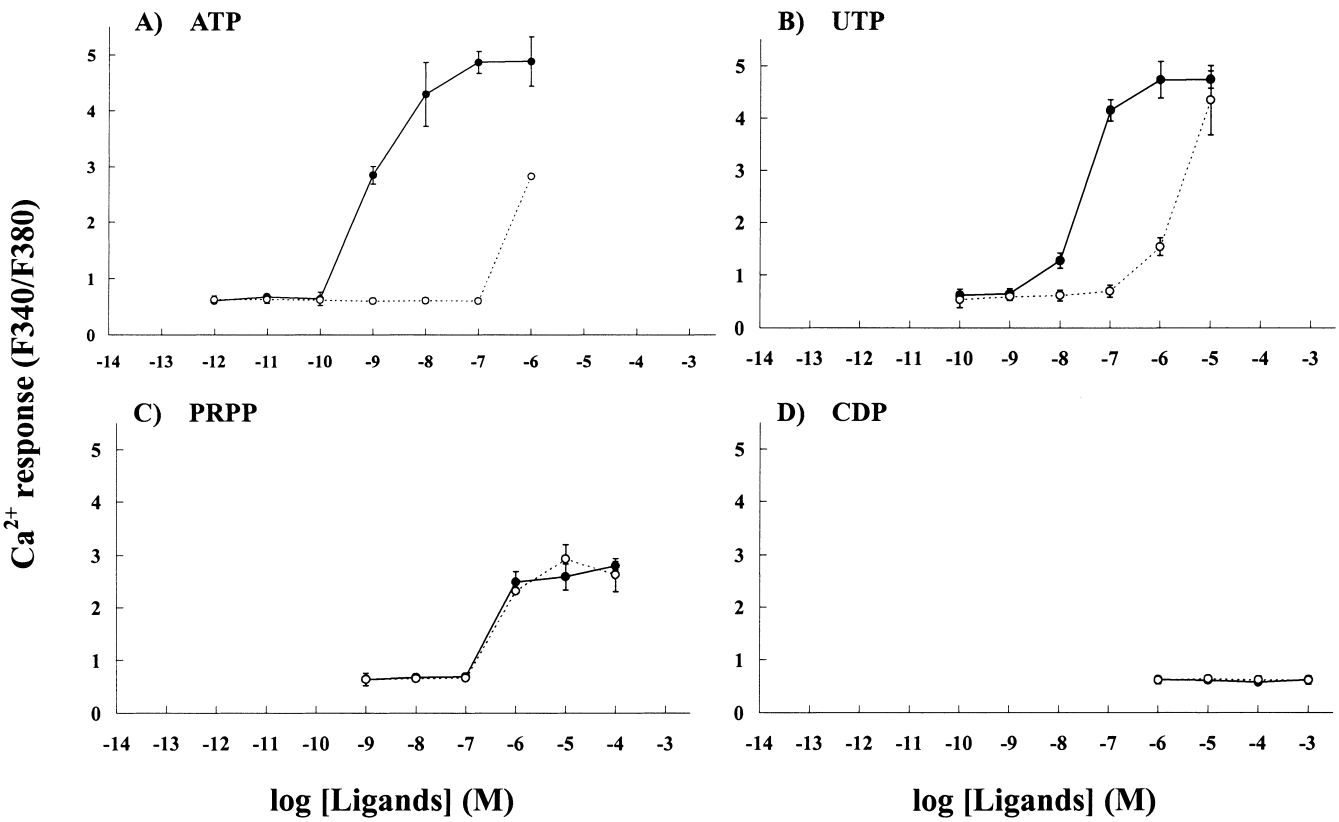

Fig. 4. Dose-response curves for ligand-evoked $[Ca^{2+}]_i$ increases via the expressed hP2Y$_2$-hGqα fusion protein. Wild-type CHO cells and CHO cells stably expressing hP2Y$_2$-hGqα fusion protein were loaded with fura-2/AM to measure changes in $[Ca^{2+}]_i$. Wild-type CHO cells (open circle) or cells transfected with the hP2Y$_2$-hGqα fusion protein (closed circle) were evoked with different concentrations of ligands, A) ATP, B) UTP, C) PRPP, and D) CDP. Individual curves represent the means ± S.E.M. of 3 – 5 experiments each measuring at least 10 single cells.

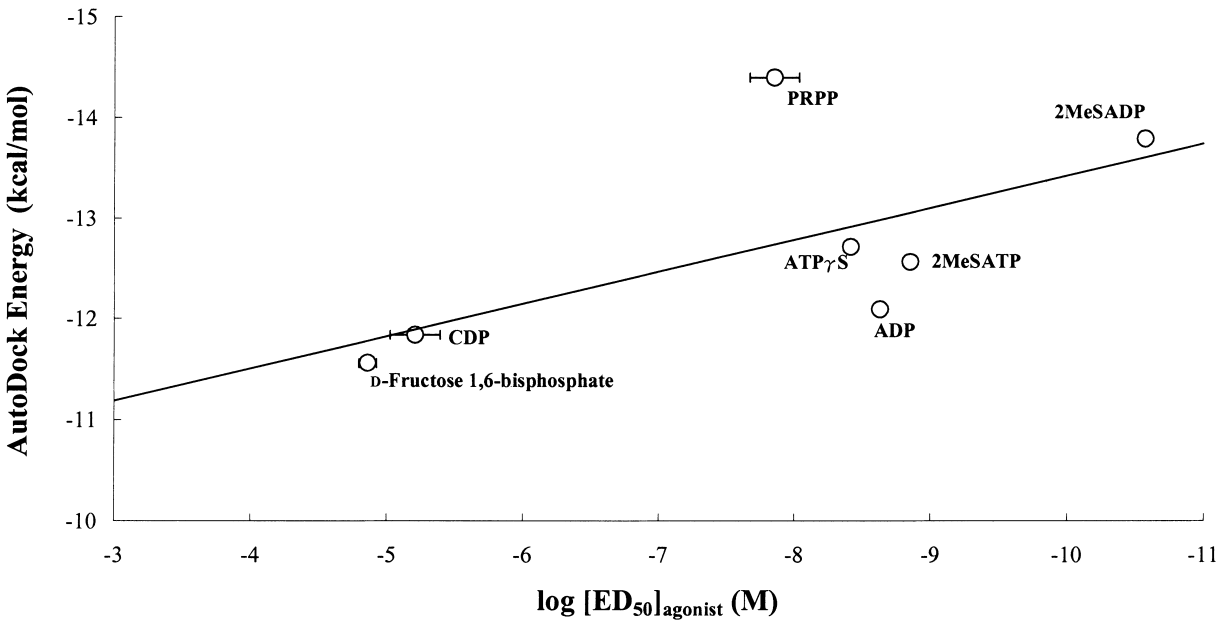

Fig. 5. Correlation between binding energies calculated by AutoDock and ED_{50} values of $[Ca^{2+}]_i$ measurements. The straight line was drawn by the least-squares method and the correlation coefficient was 0.63 (P<0.05).

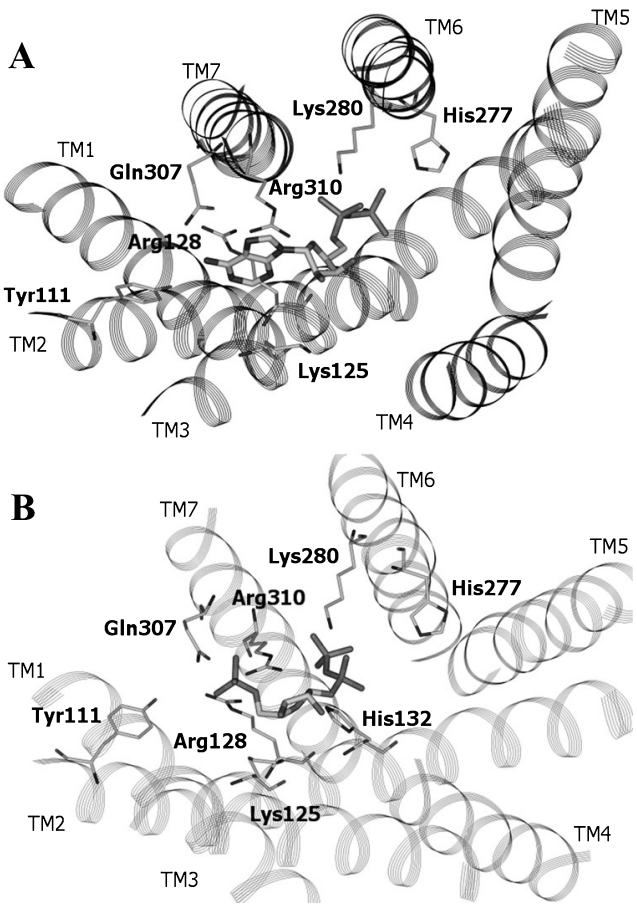

Fig. 6. 3D models of ADP- and PRPP-bound hP2Y$_1$ receptor. The side chains of the important residues in proximity to the docked ADP molecule (A) and PRPP molecule (B) are highlighted and labeled. A) Residues in proximity to the docked ADP molecule: adenine to Tyr111 and Arg310, ribose to Arg310, phosphate to Arg310 and Lys280. B) Residues in proximity to the docked PRPP molecule: 5-phosphate to Gln307 and Arg310, ribose to Arg310, 1-diphosphate to His132, Lys280, and Arg310.

O19), and Arg310/TM7 (2.01Å O11, 2.26Å O17, 2.22Å O19) (Fig. 6B).

Discussion

The number of P2Y-receptor subtypes has increased by more than ten, so that the physiological functions of these P2Y receptors are difficult to understand without specific agonists and antagonists. In addition, P2Y receptors are distributed so widely in the whole body and mammalian cell lines that the elucidation of the feature of any single subtype is difficult. In order to overcome these problems, we attempted a rational approach to identify hP2Y$_1$-specific agonists and antagonists using a sensitive in vitro assay of P2Y receptor and an in silico screening.

Recent studies showed that the receptor interacts with Gα proteins more productively when expressed as a GPCR-Gα fusion protein than when expressed as separate proteins (22). We previously reported that the hP2Y$_1$-hGqα fusion protein was highly expressed in Sf9 insect cell membranes transfected by the recombinant baculovirus anchoring the fusion protein gene. The fusion receptor protein was found to work functionally in GTPγS binding assay (23). However, since the expression in Sf9 cells was transient, we have prepared a CHO mammalian cell line that stably expresses hP2Y$_1$-hGqα fusion protein. The Flp-In^{TM} system in CHO cells was developed to provide a high expression system, by locating the insertion site of the passenger DNA into a very active genomic locus for transcription in the Flp-In^{TM} CHO cell line. We could confirm such a high expression level of the fusion protein by the RT-PCR assay. As shown in Fig. 1, the transfected cells effectively expressed the fusion protein so that the level of the hP2Y$_1$ receptor was as high as the major cytoskeleton protein β-actin.

Thus, the transfected CHO cells provided a useful tool to measure the hP2Y$_1$ receptor-mediated Ca^{2+} response. In fact, the hP2Y$_1$ agonists, ADP, 2MeSADP and 2MeSATP, evoked $[Ca^{2+}]_i$ increase in the transfected cells with the ED_{50} values of 2.2 nM of ADP, 0.026 nM of 2MeSADP, and 1.4 nM of 2MeSATP. The reported ED_{50} values of these ligands for the P2Y$_1$ receptor vary from 0.13 to 257 nM for ADP, from 0.35 to 1.27 nM for 2MeSADP, and 0.06 to 4.9 nM for 2MeSATP, depending on the materials and assay methods (24 – 28). The reason for these variations remains to be elucidated. One of the reasons is that there exist multiple P2Y subtypes in materials that complicate the quantitative analyses. However, we can expect a highly effective interaction of P2Y$_1$ receptor and Gqα protein in our assay system that can distinguish the activation of P2Y$_1$ receptor from other P2Y subtypes.

To screen the ligands for hP2Y$_1$ receptor efficiently, we have employed an in silico screening using AutoDock 3.0. The binding energy-values by AutoDock of the other neurotransmitters were between −2.39 and −5.31 kcal/mol, while those for known hP2Y$_1$ agonists and antagonists were less than −11.6 kcal/mol. These hP2Y$_1$ ligands were ranked within the top 6%. These results indicated that the screening method seemed to be successful. Thus we selected 21 compounds including known hP2Y$_1$ agonists and antagonists from the compounds in the top 6% (Table 1) and measured their activities to induce $[Ca^{2+}]_i$ increases in the transfected cells.

The hP2Y$_1$ agonists, ADP, 2MeSADP, 2MeSATP and ATPγS, showed expectedly high potency to stimu-

late $[Ca^{2+}]_i$ increases in the CHO cells expressing $hP2Y_1$ fusion receptor. PRPP, CDP, and D-fructose 1,6-bisphosphate also evoked $[Ca^{2+}]_i$ increases. Especially, PRPP was found to be more effective in activating the $hP2Y_1$ fusion receptor, with the ED_{50} value of 15 nM (Fig. 2E). The putative $hP2Y_1$-specific antagonist, A3P5PS completely blocked the 100 nM PRPP-evoked $[Ca^{2+}]_i$ increase, suggesting that PRPP acted on $P2Y_1$ receptor as an agonist (Fig. 3H). Due to the higher expression level of fusion $P2Y_1$ receptor in the transfected CHO cells, the present ED_{50} value may not reflect a value at more physiological level of expression and coupling of the receptor.

To evaluate the effect of PRPP on other P2Y receptors, we prepared CHO cells stably expressing $hP2Y_2$-hGqα fusion protein and examined if PRPP could act on the $hP2Y_2$ receptor. As a result, we observed that ATP and UTP, known agonists for the $hP2Y_2$ receptor, evoked the $[Ca^{2+}]_i$ increase more effectively in the transfected cells, while PRPP evoked moderate $[Ca^{2+}]_i$ increases in the transfected cells as well as the wild-type cells (Fig. 4: A and B). The dose-response curves obtained from the wild-type and transfected cells showed no significant difference in the responses to PRPP in the two cell-lines (Fig. 4C). The ED_{50} value was about 400 nM, which is about 30-fold higher than the values for the $hP2Y_1$ receptor. These results suggested that PRPP did not act on the $hP2Y_2$ receptor. To determine the subtype of P2Y receptors responding to PRPP in the wild-type cells, we investigated which subtypes were expressed in CHO cells by RT-PCR assay with primers designed to amplify the genes for the $P2Y_1$, $P2Y_2$, $P2Y_4$, $P2Y_6$, and $P2Y_{12}$ receptors. As a result, the $P2Y_2$, $P2Y_6$, and $P2Y_{12}$ receptors were found to be expressed with an intensity order of $P2Y_{12} \gg P2Y_6 = P2Y_2$. The agonist potency ratio of the $P2Y_{12}$ receptor has been reported as 2MeSADP > ADP, and UTP is not a $P2Y_{12}$ ligand. This ligand potency and selectivity are similar to those of the $P2Y_1$ receptor. Considering these results, it is possible to speculate that PRPP weakly acts on the $P2Y_{12}$ receptor expressed in the wild-type CHO cells.

P2X receptors commonly possess a high affinity binding motif to triphosphate adenine nucleotides, such as ATP, 2MeSATP and α,βMeATP, that shows similarities with the metal binding regions of metallothioneins and zinc finger motifs (29). This binding motif is entirely different from the ADP binding site formed by the seven transmembrane α-helices in $hP2Y_1$ receptor. Thus, the agonist binding motif in P2X receptors is not suitable for PRPP or ADP. From these results, as a temporal conclusion, we propose that PRPP is a full agonist of the $P2Y_1$ receptor and a partial agonist for the $P2Y_{12}$ receptor.

The role of PRPP has been considered to be an important compound of intermediary metabolism. It is required for the de novo biosynthesis of purine and pyrimidine nucleotides and the pyridine nucleotide coenzyme NAD, as well as for the salvage of preformed purine, pyrimidine, and pyridine bases. PRPP is also used in the synthesis of histidine and tryptophan by plants and microorganisms (30 – 34). However, there is no report that indicates PRPP exists in the extracellular space. Therefore, currently it is not clear whether PRPP is a $P2Y_1$ endogenous transmitter or modulator.

According to the literature on $P2Y_1$ ligands, some compounds such as GTP and UTP are known to have no action on the $P2Y_1$ receptor. However, the AutoDock calculation showed that they bind more strongly than 2MeSADP, the pharmacologically strongest $P2Y_1$ agonist. Our $[Ca^{2+}]_i$ assay indicated that GTP or UTP did not show any effect at the concentration of 10^{-8} M on the transfected cells; and at 10^{-7} M, it induced significant increase in the $[Ca^{2+}]_i$ in both transfected and wild type cells, preventing examination of the true effect of GTP on the $P2Y_1$ receptor. CDP at 10 μM evoked $[Ca^{2+}]_i$ increase, although in a low affinity manner (Fig. 2F), while 1 μM UDP and 100 μM UDP-glucose showed weak antagonistic effects on 10 nM ADP-evoked $[Ca^{2+}]_i$ increases (Fig. 3: D and E). Furthermore, farnesyl diphosphate was totally inactive in the range of 10^{-6} – 10^{-4} M, while it was also ranked with a lower energy score in Table 1. These facts indicated that the highly ranked compounds showing weak agonist or antagonist activities may not actually bind well to the binding sites of a potent $P2Y_1$ agonist or antagonist on the receptor.

D-Fructose 1,6-bisphosphate was ranked at the lower position in the top 6% of Table 1 and shown to act as an $hP2Y_1$ agonist (Fig. 2G), while D-fructose 2,6-bisphosphate, the structure of which is slightly distinct from D-fructose 1,6-bisphosphate, did not bind to the $hP2Y_1$ receptor. It is interesting that essentially different results were obtained for the two fructose-derivatives, in spite of the fact that the structural similarity in these compounds is very high. The results suggest that the in silico and in vitro combined approach can provide us an unexpected and useful idea to understand the pharmacophore features of $hP2Y_1$ ligands.

As shown in Fig. 5, the binding energies calculated by AutoDock and ED_{50} values of Ca^{2+} measurements showed a fairly good correlation, with a correlation coefficient of 0.63 (P<0.05). PRPP possesses a diphosphate group that effectively interacts with the binding site (TM6 and TM7) common to other known agonists, while PRPP has no adenine moiety so that the binding manner should be slightly different from those

of known agonists (Fig. 6). Moreover, PRPP comes close to the receptor more easily because PRPP is much smaller than nucleotide agonists. Thus, the gap found in PRPP in Fig. 5 may reflect these points.

A study of HIV-I protease-inhibitor also showed good correlation between experimentally determined binding energies and calculated binding energy using AutoDock (35). Their correlation coefficients were between 0.4 and 0.8. The 3D structures of HIV-I protease-inhibitor used in the study were determined by X-ray crystallography with a resolution of less than 3.0 Å. Considering this, the 0.63 correlation coefficient obtained in the present study is high enough to validate our results and to demonstrate that our 3D model was reasonable for in silico screening.

According to the ligand-bound 3D receptor models, ADP and PRPP bind to the same binding pocket in the $hP2Y_1$ receptor (Fig. 6: A and B). The docking model shows that the ribose of ADP binds to Arg310/TM7, and the alpha phosphate group also comes close to the same residue. Previously Moro et al. constructed a 3D model of a ligand-docked $P2Y_1$ receptor using ATP as a ligand (36). In the present study, we used the endogenous agonist ADP to make a similar 3D model. Due to the different ligands used, there is an inconsistency between the two models: the beta phosphate group interacts with Arg310 in their model but alpha phosphate interacts with Arg310 in our model. In addition, we constructed the model by employing a hybrid method (as mentioned in the introduction), but they used a simple homology modeling. Considering these points, we should not directly compare the two models. Nevertheless, there exists an important agreement in that the Arg310 interacts with two groups, a phosphate group and adenine moiety of adenine nucleotides. They have reported that the ribose moiety of adenosine nucleotides played an important role for the $P2Y_1$-receptor activation, while it was not essential for recognition of antagonists by the receptor (37). The ribose can be replaced by a pseudosugar ring such as the carbocyclic ring (37). Our model also demonstrated that ribose-modified ADP still showed significantly low AutoDock energies, −13.05 kcal/mol for dideoxy ribose and −12.84 kcal /mol for a pseudosugar ring. Moreover, they showed that (*N*)-methanocarbo modification of the ribose moiety of 2MeSADP exhibited a higher potency as a $P2Y_1$ agonist than the (*S*)-isomer (38). This tendency was also found by our AutoDock calculation. That indicated (*N*)-methanocarbo modification of the ribose moiety of ADP revealed a lower docked energy than the (*S*)-isomer, namely, −12.33 and −8.30 kcal/mol, respectively. Thus, our results are well consistent with their reports.

According to the PRPP-docked $P2Y_1$ receptor 3D model, the 5-phosphate of the PRPP molecule interacts with Gln307/TM7 and Arg310. The diphosphate group of PRPP interacts with Arg310, Lys280/TM6, and His132/TM3. These results suggest that the 5-phosphate of PRPP like the adenine moiety of ADP.

Suramin and PPADS, which have no bases, have been known to bind to the $hP2Y_1$ receptor as a non-specific P2 antagonist. However an agonist that has no base has not been found. Generally, the bases of nucleotides are considered to be required to activate P2Y receptors and to make the selectivity of various P2Y-receptor subtypes. Many studies of drug design were based on the adenine molecule (36 – 40). Surprisingly, PRPP has selectivity to the $P2Y_1$ receptor as shown in this paper, although PRPP has only a ribose and three phosphates. This fact suggests that we would be able to design an agonist with no adenine moiety in a novel drug design for the $P2Y_1$ receptor. In addition, we would be able to design a specific antagonist of $P2Y_1$ receptor based on the PRPP molecule. This is an important point since the specific antagonists of the $P2Y_1$ receptor as well as the $P2Y_{12}$ receptor are expected to be medicines for thrombosis through the inhibition of ADP-induced human platelet aggregation (26, 41).

Finally, the studies shown in the present paper could lead to development of a novel drug design for the P2Y receptor family. As far as we know, this is the first report in which the surrogate ligands for the $hP2Y_1$ receptor were rationally identified by in silico screening and in vitro assay. Accumulation of these data is indispensable not only to refine the 3D structure of $P2Y_1$ receptor but also to develop a computational method to elucidate the mechanism by which a ligand binds to a GPCR.

Acknowledgment

We would like to thank to Dr. E. Cooper of Ritsumeikan University (Kusatsu, Shiga) for help in preparing this manuscript.

References

1 Muller G. Towards 3D structures of G protein-coupled receptors: multidisciplinary approach. Curr Med Chem. 2000;7:861–888.

2 Palczewski K, Kumasaka T, Hori T, et al. Crystal structure of rhodopsin: a G protein-coupled receptor. Science. 2000;289: 739–745.

3 Bowie JU. Helix-bundle membrane protein fold templates. Protein Sci. 1999;812:2711–2719.

4 Koshi JM, Bruno WJ. Major structural determinants of transmembrane proteins identified by principal component analysis. Proteins. 1999;3:333–340.

5 Pilpel Y, Ben-Tal N, Lancet D. kPROT: a knowledge-based scale for the propensity of residue orientation in transmembrane segments. Application to membrane protein structure prediction. J Mol Biol. 1999;4:921–935.

6 Hirokawa T, Uechi J, Sasamoto H, Suwa M, Mitaku S. A triangle lattice model that predicts transmembrane helix configuration using a polar jigsaw puzzle. Protein Eng. 2000;11:771–778.

7 Overington J, Donnelly D, Johnson MS, Sali A, Blundell TL. Environment-specific amino acid substitution tables: tertiary templates and prediction of protein folds. Protein Sci. 1992; 2:216–226.

8 Donnelly D, Overington JP, Blundell TL. The prediction and orientation of α-helices from sequence alignments: the combined use of environment-dependent substitution tables, Fourier transform methods and helix capping rules. Protein Eng. 1994;5:645–653.

9 Hiramoto T, Kikuchi T, Fujita N. Prediction of 3D structure and ligand binding sites in purinoceptors. Memoirs of the Institute of Science & Engineering, Ritsumeikan University 60. 2001:47–57. (text in Japanese with English abstract)

10 Hiramoto T, Nemoto W, Kikuchi T, Fujita N. Construction of hypothetical three-dimensional structure of $P2Y_1$ receptor based on Fourier transform analysis. J Protein Chem. 2002;8:537–545.

11 Goodsell DS, Olson AJ. Automated docking of substrates to proteins by simulated annealing. Proteins. 1990;3:195–202.

12 Morris GM, Goodsell DS, Huey R, Olson AJ. Distributed automated docking of flexible ligands to proteins: parallel applications of AutoDock 2.4. J Comput Aided Mol Des. 1996;4:293–304.

13 Morris GM, Goodsell DS, Halliday RS, et al. Automated docking using a Lamarckian genetic algorithm and an empirical binding free energy function. J Comp Chem. 1998;19:1639–1662.

14 Goodsell DS, Lauble H, Stout CD, Olson AJ. Automated docking in crystallography: analysis of the substrates of aconitase. Proteins. 1993;1:1–10.

15 Lunney EA, Hagen SE, Domagala JM, et al. A novel nonpeptide HIV-1 protease inhibitor: elucidation of the binding mode and its application in the design of related analogs. J Med Chem. 1994;17:2664–2677.

16 Gieldon A, Kazmierkiewicz R, Slusarz R, Ciarkowski J. Molecular modeling of interactions of the non-peptide antagonist YM087 with the human vasopressin V1a, V2 receptors and with oxytocin receptors. J Comput Aided Mol Des. 2001; 15:1085–1104.

17 Abbracchio MP, Burnstock G. Purinoceptors: are there families of P2X and P2Y purinoceptors? Pharmacol Ther. 1994;64:445–475.

18 Burnstock G, King BF. Numbering of cloned P2 purinoceptors. Drug Dev Res. 1996;38:67–71.

19 Abbracchio MP, Boeynaems JM, Barnard EA, et al. Characterization of the UDP-glucose receptor (re-named here the $P2Y_{14}$ receptor) adds diversity to the P2Y receptor family. Trends Pharmacol Sci. 2003;24:52–55.

20 Barnard EA, Simon J, Webb TE. Nucleotide receptors in the nervous system. An abundant component using diverse transduction mechanisms. Mol Neurobiol. 1997;15:103–129.

21 Hollopeter G, Jantzen HM, Vincent D. Identification of the platelet ADP receptor targeted by antithrombotic drugs. Nature. 2001;409:202–207.

22 Seifert R, Lee TW, Lam VT, Kobilka BK. Reconstitution of β2-adrenoceptor-GTP-binding-protein interaction in Sf9 cells – high coupling efficiency in a β2-adrenoceptor-Gsα fusion protein. Eur J Biochem. 1998;255:369–382.

23 Fujita N, Yamamoto Y, Murakami T, Hiramoto T. Characterization of fusion protein between purinoceptor and Gα proteins. Pharmacologist. 2002;442;144.

24 Vohringer C, Schafer R, Reiser G. A chimeric rat brain P2Y1 receptor tagged with green-fluorescent protein: high-affinity ligand recognition of adenosine diphosphates and triphosphates and selectivity identical to that of the wild-type receptor. Biochem Pharmacol. 2000;59:791–800.

25 Boyer JL, Romero-Avila T, Schachter JB, Harden TK. Identification of competitive antagonists of the $P2Y_1$ receptor. Mol Pharmacol. 1996;50:1323–1329.

26 Jiang Q, Guo D, Lee BX, et al. A mutational analysis of residues essential for ligand recognition at the human $P2Y_1$ receptor. Mol Pharmacol. 1997;52:499–507.

27 Hoffmann C, Moro S, Nicholas RA, Harden TK, Jacobson KA. The role of amino acids in extracellular loops of the human $P2Y_1$ receptor in surface expression and activation processes. J Biol Chem. 1999;274:14639–14647.

28 Schachter JB, Harden TK. An examination of deoxyadenosine 5'(α-thio)triphosphate as a ligand to define P2Y receptors and its selectivity as a low potency partial agonist of the $P2Y_1$ receptor. Br J Pharmacol. 1997;121:338–344.

29 Freist W, Verhey JF, Stuhmer W, Gauss DH. ATP binding site of P2X channel proteins: structural similarities with class II aminoacyl-tRNA synthetases. FEBS Lett. 1998;434:61–65.

30 Hove-Jensen B. Phosphoribosylpyrophosphate (PRPP) – less mutants of *Escherichia coli*. Mol Microbiol. 1989;3:1487–1492.

31 Khorana HG, Fernandes JF, Kornberg A. Pyrophosphorylation of ribose 5-phosphate in the enzymatic synthesis of 5-phosphorylribose 1-pyrophosphate. J Biol Chem. 1958;230:941–948.

32 Switzer RL. Regulation and mechanism of phosphoribosylpyrophosphate synthetase. I. Purification and properties of the enzyme from *Salmonella typhimurium*. J Biol Chem. 1969; 244:2854–2863.

33 Switzer RL, Sogin DC. Regulation and mechanism of phosphoribosylpyrophosphate synthetase. V. Inhibition by end products and regulation by adenosine diphosphate. J Biol Chem. 1973;248:1063–1073.

34 Tatibana M, Kita K, Taira M, et al. Mammalian phosphoribosylpyrophosphate synthetase. Adv Enzyme Regul. 1995;35:229–249.

35 Jenwitheesuk E, Samudrala R. Improved prediction of HIV-1 protease-inhibitor binding energies by molecular dynamics simulations. BMC Struct Biol. 2003;3:2.

36 Moro S, Hoffmann C, Jacobson KA. Role of extracellular loops of G-protein-coupled receptors in ligand recognition: a molecular modeling study of the human $P2Y_1$ receptor. Biochemistry. 1999;38:3498–3507.

37 Kim YC, Gallo-Rodriguez C, Jang SY, et al. Acyclic analogues of deoxyadenosine 3',5'-bisphosphate as $P2Y_1$ receptor antagonists. J Med Chem. 2000;43:746–755.

38 Nandanan E, Jang SY, Moro S, et al. Synthesis, biological activity, and molecular modeling of ribose-modified deoxyadenosine bisphosphate analogues as $P2Y_1$ receptor ligands. J Med Chem. 2000;43:829–842.

39 Waldo GL, Corbitt J, Boyer JL, et al. Quantitation of the $P2Y_1$ receptor with a high affinity radiolabeled antagonist. Mol Pharmacol. 2002;62:1249–1257.

40 Boyer JL, Adams M, Ravi RG, Jacobson KA, Harden TK. 2-Chloro *N*(6)-methyl-(*N*)-methanocarba-2'-deoxyadenosine-3',5'-bisphosphate is a selective high affinity $P2Y_1$ receptor antagonist. Br J Pharmacol. 2002;135:2004–2010.

41 Nicholas RA. Identification of the $P2Y_{12}$ receptor: a novel member of the P2Y family of receptors activated by extracellular nucleotides. Mol Pharmacol. 2001;60:416–420.